

## Article

# A 3D-Printed Enclosed Twist Dielectric Resonator Antenna with Circular Polarization

Andrea Ávila-Saavedra <sup>1,†</sup>, Marcos Diaz <sup>2,†</sup> and Francisco Pizarro <sup>1,\*,†</sup>

<sup>1</sup> Escuela de Ingeniería Eléctrica, Pontificia Universidad Católica de Valparaíso, Valparaíso 2362804, Chile; andrea.avila.s@mail.pucv.cl

<sup>2</sup> Space and Planetary Exploration Laboratory (SPEL), Departamento de Ingeniería Eléctrica, Facultad de Ciencias Físicas y Matemáticas, Universidad de Chile, Santiago 8370458, Chile; mdiazq@ing.uchile.cl

\* Correspondence: francisco.pizarro.t@pucv.cl

† These authors contributed equally to this work.

**Abstract:** This article presents a circular polarized enclosed dielectric resonator antenna (DRA), operating at 5.8 GHz. The design consists of a twist DRA, which is enclosed in a box to give stability to the structure. The circular polarization of the antenna depends on the sense of twisting the top with respect to its base to achieve Left Hand Circular Polarization (LHCP) or Right Hand Circular Polarization (RHCP). The antenna was manufactured using 3D printing and low-loss dielectric filament. The measurement results show the two resonance frequencies and an axial ratio below 3 dB at the operational frequency, while exhibiting a bandwidth and gain compatible for unmanned aerial vehicle (UAV) applications.

**Keywords:** dielectric resonator antenna; circular polarization; 3D printing



Academic Editors: Giovanni Maria Sardi and Walter Fuscaldo

Received: 8 December 2024

Revised: 11 January 2025

Accepted: 13 January 2025

Published: 20 January 2025

**Citation:** Ávila-Saavedra, A.; Diaz, M.; Pizarro, F. A 3D-Printed Enclosed Twist Dielectric Resonator Antenna with Circular Polarization. *Appl. Sci.* **2025**, *15*, 992. <https://doi.org/10.3390/app15020992>

**Copyright:** © 2025 by the authors. Licensee MDPI, Basel, Switzerland. This article is an open access article distributed under the terms and conditions of the Creative Commons Attribution (CC BY) license (<https://creativecommons.org/licenses/by/4.0/>).

## 1. Introduction

In recent years, additive manufacturing has gained huge interest in microwave and antenna research [1]. This is mainly due to the possibility of manufacturing prototypes or functional parts that were either too expensive or difficult to implement using standard fabrication processes. This is also possible due to the introduction of conductive filaments and low-loss dielectric filaments [2] and the lower cost of high-resolution 3D printers; this combination makes these solutions appear cost-effective for several applications [3]. Some topologies that have been implemented are metamaterials [4,5], horn antennas [6], dielectric lenses [7], and other structures [8,9].

One particular kind of antenna that has been directly taking advantage of 3D printing is dielectric resonator antennas (DRAs). These antennas, which consist of a dielectric slab that can radiate depending on how it is excited, offer significant versatility in terms of radiation patterns and operational frequencies [10]. This is thanks to the possibility of exciting different cavity modes in the dielectric structure, which are dependent on the shape of the slab, its dimensions and its permittivity. One of the drawbacks of this technology is the possible choice of materials for the dielectric slab, in that the permittivities are basically set by the ceramic or dielectric in use. In addition, difficult shapes can be expensive or difficult to implement, for example, when using ceramic materials for high-permittivity values, which can limit the kind of topologies that can be implemented. Both issues can be solved by using 3D printing and the aforementioned dielectric filaments [11].

The versatility of DRAs is also important when implementing circular polarized (CP) antennas. This characteristic has been used in wireless communication applications, such as

satellite communications and unmanned vehicles [12], for the advantages that are offered regarding the reduction in the delay spread [13] and its robustness in the face of multipath interference [14,15]. From that perspective, few works have explored implementing CP 3D-printed DRA. Amongst those works, we can find a cylindrical DRA that includes a parasitic helix to achieve CP [16], and others that use an integrated polarizer [17,18].

This manuscript presents an enclosed twist DRA that generates a CP depending on the turning sense of the twist. The antenna operates at 5.8 GHz and is a single-fed structure, which makes it easier for implementation. Preliminary simulation studies were presented in [19], and this work shows a final design, modal analysis, and the manufacturing and measurement results of the antenna.

## 2. Dielectric Resonator Antenna Design and Parametric Studies

The proposed antenna design is based on a rectangular DRA fed with a single-aperture couple feeding. This feeding network will excite a TE mode [20], which gives a radiation pattern compatible with the intended UAV applications. The drawback of using this single feeding technique is that this configuration makes the antenna radiated with a linear polarization, which is not the best for the target application. As a CP polarization is needed, we proceed to modify the structure of the DRA in order to keep a simple feeding technique.

### 2.1. Twist DRA Design

The main object of the antenna corresponds to a twisted rectangular DRA to obtain CP. The twist consists of four stepped rectangular DRAs [21] that are rotated sequentially and then joined together to obtain the twist geometry. This structure will excite two orthogonal modes that will generate a CP on the desired operational frequency [22,23]. We proceed then to realize two parametric studies: one regarding the inner box dimensions and the other regarding the top rotation of the twist, as shown in Figure 1. For all the cases, the top box is rotated  $\theta$  degrees with respect to the bottom box, while the other boxes are rotated sequentially in an equally spaced degree increment. Finally, all boxes are connected through their vertices of the upper faces so as to obtain the twisted DRA. The relative permittivity used for this structure is  $\epsilon_{r1} = 13$ .

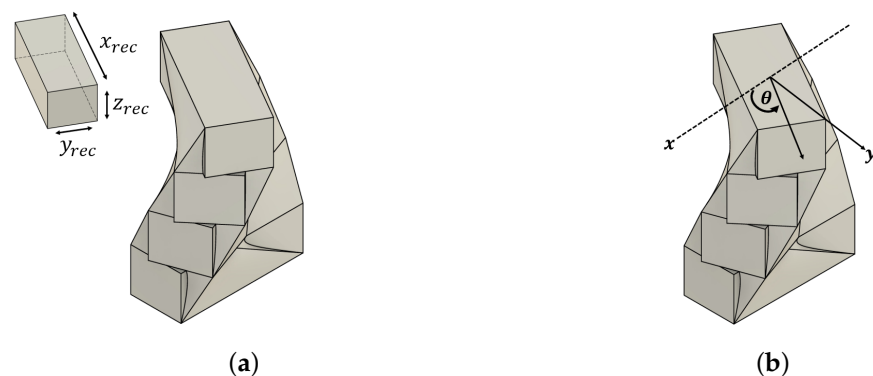


**Figure 1.** Schematic of the proposed antenna. (a) Dimension of the rectangles. (b) Rotation of the rectangles.

As this design has several variables that can affect the behavior of the antenna, most notably the inner box size and rotation between the structures, we proceed to conduct a parametric study of these variables using the software, ANSYS HFSS 2023 R1. The first parameter that was studied is the size of the inner rectangles in order to establish the lower dimensions suitable for exciting the required modes. Figure 2a shows the reflection coefficient  $|S_{11}|$  in dB as a function of the frequency while changing the size of the inner box. For this study, we keep a rotation of  $\theta = 60$  degrees of the top box with respect

to the bottom box. Note that we kept the height of the box  $z_{rect}$  at a constant value, as this structure is intended for using as minimal a height space as possible in the target application. As expected, the inner dimensions of the boxes have a direct impact on the frequency behavior of the DRA by shifting the resonant frequencies of the generated modes. From these variations, even if for DRAs the resulting resonance can be achieved by a form factor, we can see that  $y_{rect}$  has the larger influence over the resonance frequency due to the nature of the excitation [10]. The resulting axial ratio, shown in Figure 3, follows the same tendency in terms of frequency shift.

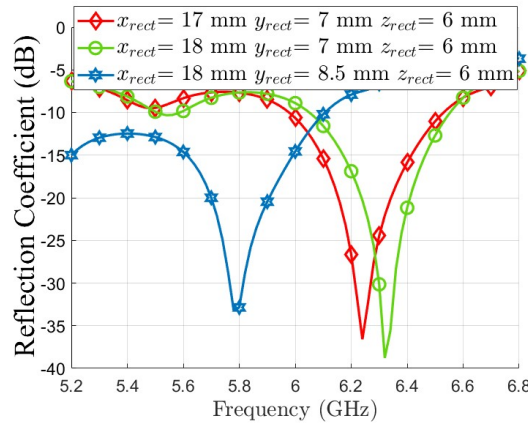


**Figure 2.** Parametric study of the reflection coefficient  $|S_{11}|$  in dB as a function of the frequency and the inner box dimensions for the twist.

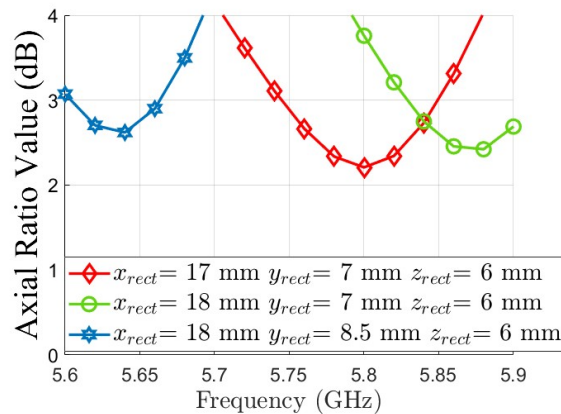


**Figure 3.** Axial ratio in dB as a function of the frequency and the inner box dimensions for the twist.

The second study is regarding the rotation of the top box in relation to the bottom of the antenna. The operation of the antenna is completely dependent on this rotation angle with respect to the x-y axis. Each rectangle is rotated by the same angle with respect to the previous one, so that the last rectangle will be rotated by  $3\theta$ , as shown in Figure 1b. We will limit this rotation to a maximum of 30 degrees, meaning that the top rectangle would have a rotation of 90 degrees with respect to the x-y axis. For this parametric study, the chosen values for the rectangle are as follows:  $x_{rect} = 17$  mm,  $y_{rect} = 7$  mm and  $z_{rect} = 6$  mm. In Figures 4 and 5, the sensitivity of the antenna for the reflection coefficient and axial ratio with respect to the rotation angle is shown. We can see that we must have a compromise between the axial ratio and matching the antenna for different angles of the structure.

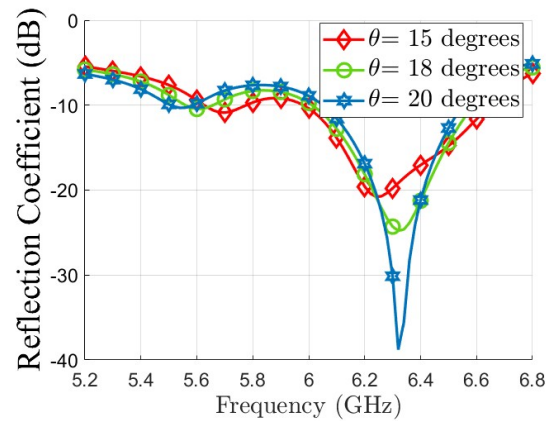


**Figure 4.** Reflection coefficient  $|S_{11}|$  as a function of the frequency for the twist implementations.

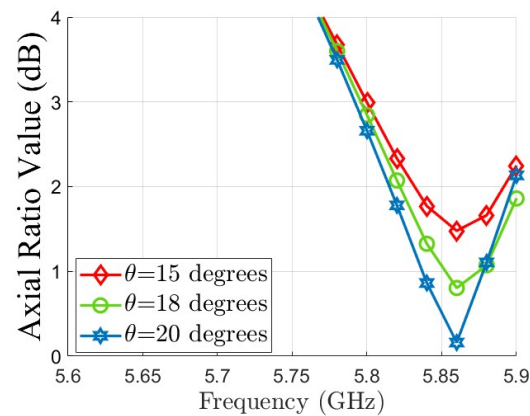


**Figure 5.** Axial ratio as a function of the frequency for the twist implementations for different rotation angles.

## 2.2. Twist with Box

The twist structure itself can have mechanical issues in implementation due to its stability and fragility. To overcome this, a dielectric box was added which has a relative permittivity  $\epsilon_{r2} = 2$  so as to be as transparent as possible, but also to ensure a good rigidity when using 3D printing, in terms of infill percentage, in order to obtain that permittivity. The schematic of the box and its dimensions are shown in Figure 6.

To obtain the final dimensions of the box, a parametric study is conducted for its different dimensions. These results are shown in Figure 7. To reduce the probability of printing errors, we first fixed the height of the box at 1 mm higher than the four stacked rectangles, reaching a total  $h_{box} = 25$  mm. Second, regarding the rotation of the inner boxes, an angle of  $\theta = 20$  degrees was chosen based on the conducted parametric studies, giving a good compromise between the matching and the axial ratio when including an outer dielectric box. Finally, the box dimensions are set to  $x_{box} = y_{box} = 19$  mm because of the resulting axial ratio achieved with these values.

## 2.3. Final Antenna Design

The final design of this antenna is a twist structure that will be created with four rectangles: a structure that will be responsible for changing the behavior of the fields, creating two orthogonal modes in the structure which allows for having CP. A schematic of the antenna and a detail of the feeding network are shown in Figure 8.

The twisted DRA is implemented using a relative permittivity of  $\epsilon_{r1} = 13$ , which corresponds to the a measured relative permittivity of the filament ABS1500 from AVIENT using our printers with a 100% infill. The dimensions of the twist antenna are a height

of  $h_{DRA} = 24$  mm, a width of  $w_{DRA} = 7$  mm, and a length of  $l_{DRA} = 17$  mm, while the top part of the DRA is rotated  $\theta_r = 60^\circ$  to achieve Left Handed Circular Polarization (LHCP). The dimensions of the antenna are set to radiate at 5.8 GHz.

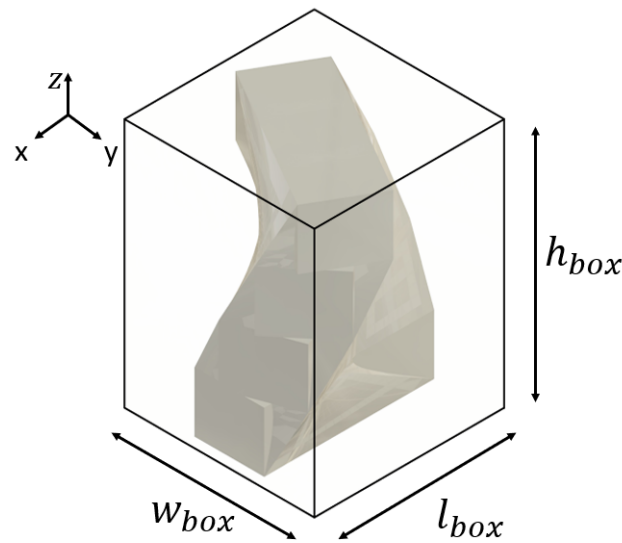


Figure 6. Schematic of the proposed antenna twist with box.

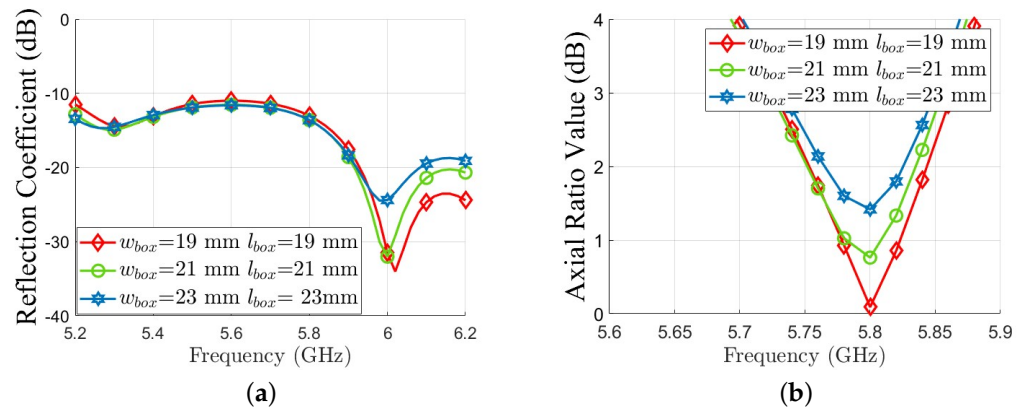


Figure 7. Parametric study of the twist with box using different lateral dimensions. (a) Reflection coefficient  $|S_{11}|$  as a function of the frequency. (b) Axial ratio as a function of the frequency.

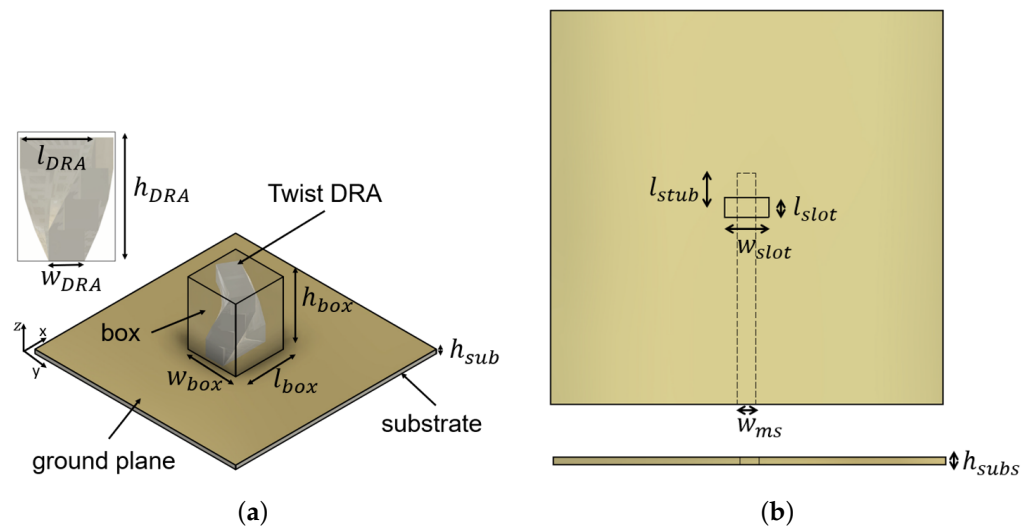


Figure 8. Schematic of the proposed antenna. (a) Twist DRA with enclosure. (b) Feeding network detail.

As this antenna is intended for UAV applications, it is important to make it as robust as possible in terms of mechanical stability. For that, the twist antenna itself can be hard to implement as a stand-alone, as it will need an additional supporting structure. For that purpose, a box that completely encloses the twisted DRA is designed, which affects the original parameters as little as possible in terms of the radiation of the antenna. For this box, a relative permittivity of  $\epsilon_{r2} = 2$  is used. This permittivity will be achieved by varying the infill percentage of the filament [24], in order to make just a one-piece implementation. The lateral dimensions of the box are a height  $h_{box} = 25$  mm, a width  $w_{box} = 19$  mm and a length  $l_{box} = 19$  mm.

Finally, for the feeding network, an aperture slot-coupling is used. The substrate used is a ROGERS RO4003 ( $\epsilon_r = 3.38$ ,  $\tan \delta = 0.0027$ ) with a height of  $h_{sub} = 1.52$  mm. The slot dimensions are a width  $w_{slot} = 9$  mm and a length of  $l_{slot} = 4$  mm. Finally, the  $50 \Omega$  microstrip line used for the coupling has a width of  $W_{ms} = 3.4$  mm and a stub length of  $l_{stub} = 7$  mm.

### 3. Simulation Results

The LHCP version of the antenna was simulated using the full-wave software, ANSYS HFSS. Figure 9 shows the simulated results of the reflection coefficient and axial ratio as a function of the frequency.

From Figure 9, we can see that the antenna is matched in the operational frequency of 5.8 GHz, with a bandwidth of 130 MHz. From the behavior of the  $|S_{11}|$ , we can see the presence of two resonant frequencies, which is typical for these kind of antennas where two orthogonal modes are excited. It is necessary to identify the modes and corroborate their orthogonality. For that, the simulated electric field vector is shown in Figure 10. From the simulated results, we can clearly see that the first resonant mode with a resonance frequency around 5.3 GHz is orthogonal to the second mode generated around 6.0 GHz; we expect that around 5.8 GHz, both modes will have a similar intensity, but with orthogonal vectors. We can confirm this behavior with the simulated axial ratio, shown in Figure 9b, where we can see that around 5.8 GHz, the axial ratio value reaches a minimum of 0 dB, confirming the CP nature of the structure.

Finally, Figure 11 shows the gain radiation pattern on two cut planes of the antenna ( $x - z$  and  $y - z$ ). The obtained radiation pattern is suitable for UAV applications in terms of its beamwidth, exhibiting a maximum of 6.7 dBi.

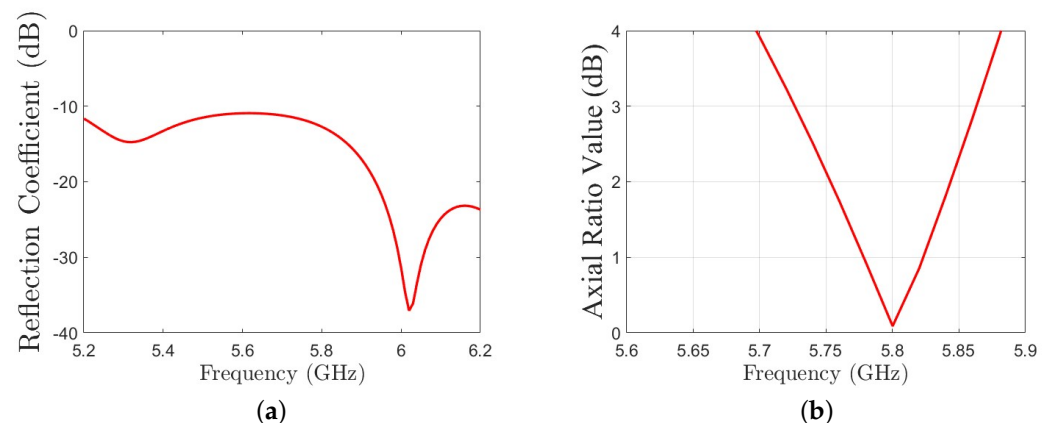


**Figure 9.** Simulation results for the LHCP implementation. (a) Reflection coefficient  $|S_{11}|$  as a function of the frequency. (b) Axial ratio as a function of the frequency.

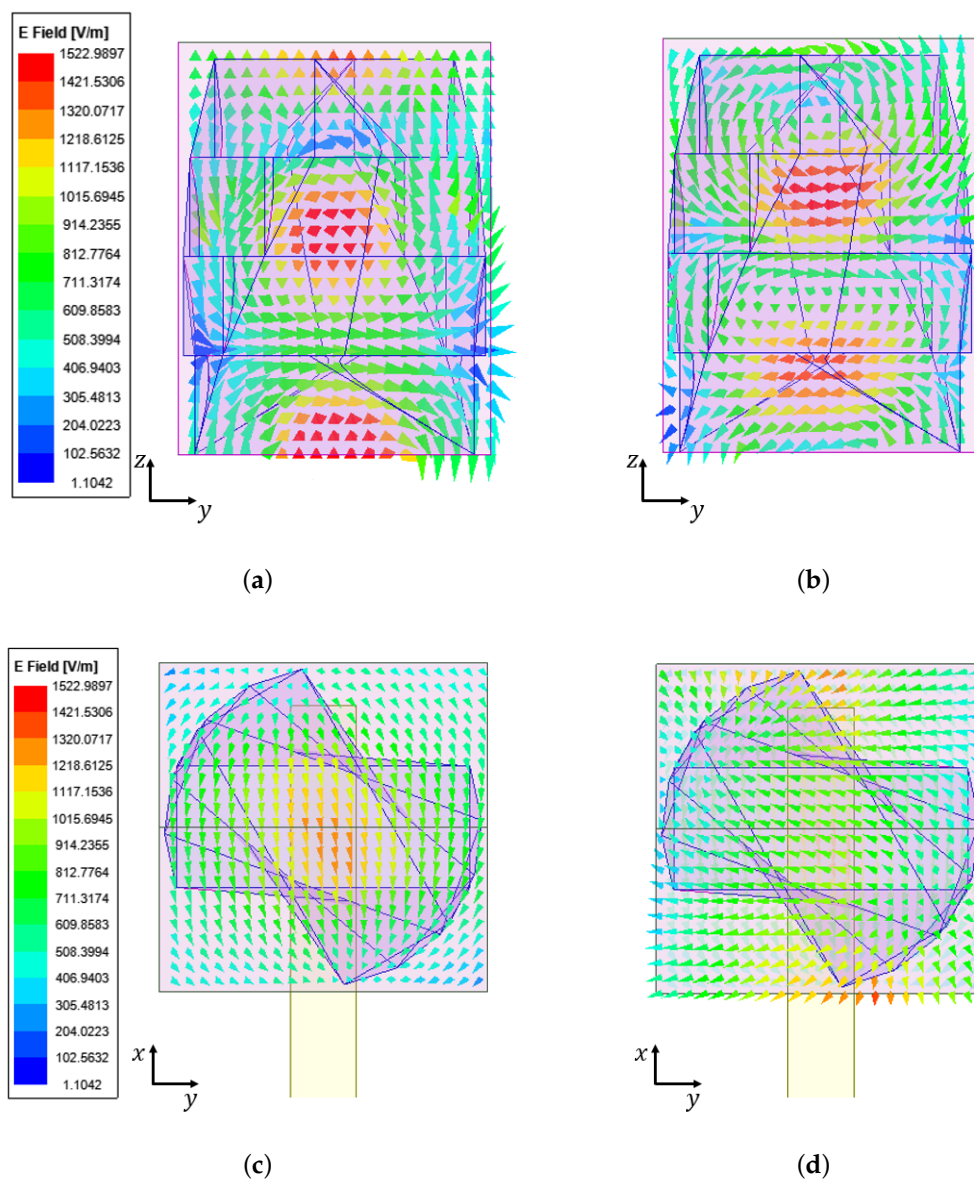


**Figure 10.** Simulated electric field distribution in the center of the DRA and a cut-side view. (a) Side view at 5.3 GHz. (b) Side view at 6.0 GHz. (c) Top view at 5.3 GHz. (d) Top view at 6.0 GHz.

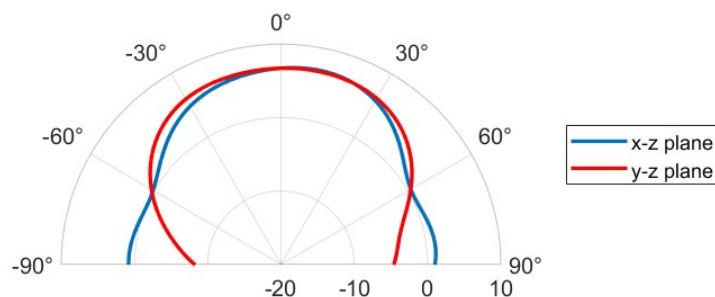


**Figure 11.** Simulated gain radiation pattern at 5.8 GHz for the LHCP implementation.

#### 4. Antenna Manufacturing Using 3D Printing

The antenna was manufactured using a Creality CP-01 printer and using the AVIENT ABS1500 filaments, with a relative permittivity of  $\epsilon_r = 15$  and a loss tangent of  $\tan \delta = 0.0010$ . The printing parameters used for this implementation are shown in Table 1.

**Table 1.** Printing parameters.

Parameter	Value
Printing Temperature	260 °C
Build Plate Temperature	90 °C
Printing Speed	20 (mm/s)
Flow	100%
Infill Percentage Twist	100%
Infill Percentage Box	10%

One notable advantage of this antenna design is its manufacturability in a single print, achieved by adjusting the infill percentage during the printing process. By varying the infill, the design enables the controlled tuning of the relative permittivity without the need for multiple fabrication steps or additional materials. For this specific implementation, a low infill percentage was used within the outer box of the antenna to minimize material usage while still meeting the functional requirements.

To assess the dielectric properties of the printed material under actual fabrication conditions, a characterization process was conducted, considering the tolerances and limitations inherent to the printer. This characterization was performed using the Nicolson–Ross–Weir (NRW) method [25], which provides an effective way to measure complex permittivity values across a defined frequency range. Test samples were analyzed within the frequency range of 4.8 GHz to 7 GHz using a WR159 waveguide setup.

Through this method, the measured relative permittivity of the ABS1500 material was found to be  $\epsilon_r = 13$  when printed with a 100% infill density, utilizing the same printer and parameters outlined in the design. These measurements confirm that, while the manufacturer specifies a relative permittivity of 15, variations in printing parameters can significantly impact the dielectric properties of the material, emphasizing the importance of in situ characterization for precision applications in high-frequency designs.

As previously described, two different permittivity values were used for the different components of the antenna. To realize this variation in permittivity while using only a single type of filament, two different infill percentages were applied, as indicated in Table 1. By modifying the infill percentage, we effectively altered the density of the material, which in turn adjusts its dielectric properties.

The slicing software UltiMaker CURA 5.7.1 was used to implement these varying infill percentages. Figure 12a illustrates the CURA interface, where different infill percentages are assigned to the different antenna regions. The final, fully fabricated antenna can be seen in Figure 12b. In this we can see, just for visualization, the different sections of the antenna. First, we see a printed version of the twist without the box, which shows how the printer implements the main radiating structure. Then, there is a version where we can see both the box and twist in the same printing process in order to confirm the compatibility of the printing process and, finally, the full enclosed twist structure. This approach not only simplifies the manufacturing process by using a single filament type but also enhances material efficiency and design flexibility, ensuring that the antenna meets

specific performance requirements without the need for additional materials or complex assembly procedures.

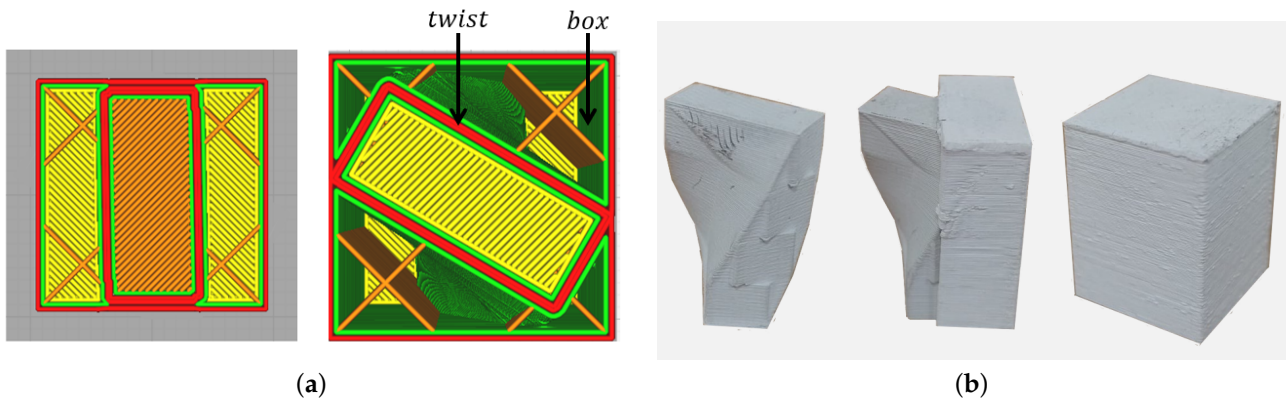


**Figure 12.** The 3D-printed antenna. (a) CURA implementation with the infill percentages. (b) Implemented antenna. From left to right: twist alone, twist in the enclosure with the exposed half, and full antenna.

## 5. Measurement Results

The measured reflection coefficient and axial ratio values are presented in Figure 13. These results indicate that the antenna is well matched to the design frequency of 5.8 GHz, showing good agreement with the simulation results. From Figure 13, we can see that the axial ratio remains below 3 dB. However, there was an increment in the dB value of the axial ratio, reaching a value of 2.6 dB at the operational frequency. The measurement of the normalized gain pattern is presented in Figure 14. We can see a deformation of the radiation pattern, while the maximum gain is reduced 2.4 dB.

One of the challenges of working with sensitive structures such as DRAs is that any small disturbance affects their operation. Therefore, a study was carried out to evaluate the sensitivity of the antenna in relation to its position with respect to the feed slot. For this, in Figure 15, we set the variable “*a*”, which will represent the movement of the position with respect to the feed. In Figure 16a, the axial ratio shows how sensitive the antenna is to a small leveling movement relative to the slot. The approximate distance the antenna moved from the central axis was measured with a vernier caliper, in this case with a value of 2 mm, which has a great influence on the axial ratio parameter and therefore on the radiation pattern.

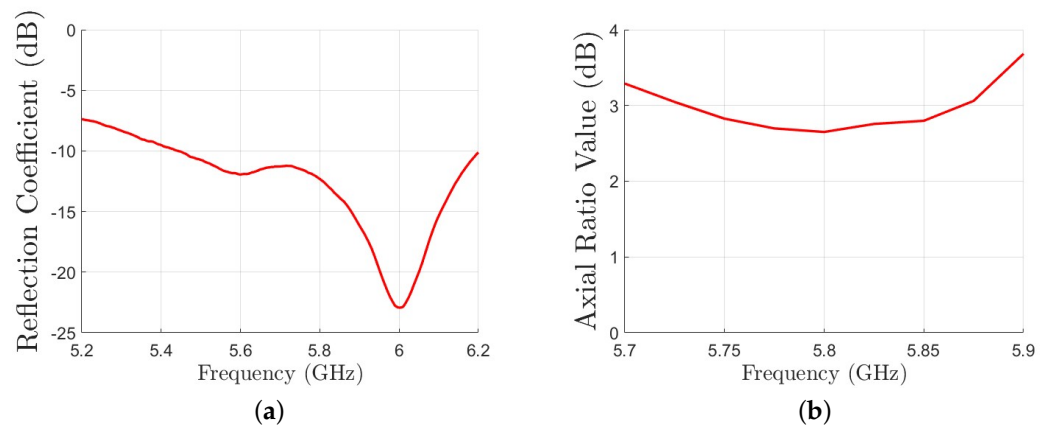


**Figure 13.** Measurement results for the LHCP implementation. (a) Reflection coefficient  $|S_{11}|$  as a function of the frequency. (b) Axial ratio as a function of the frequency.

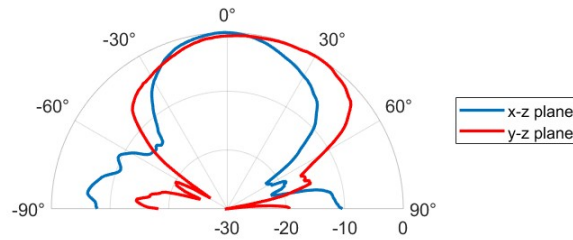


Figure 14. Results of the measured radiation pattern for the implementation of the LHCP implementation.

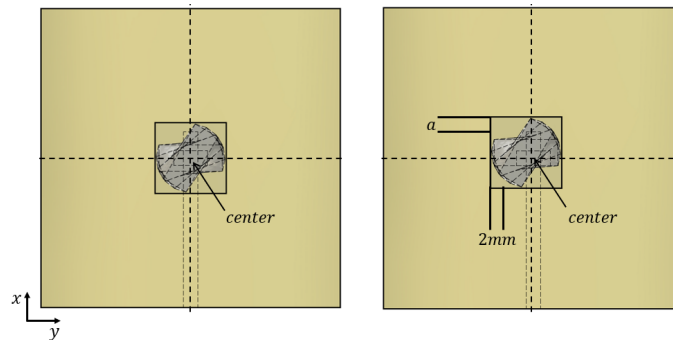


Figure 15. Top view of the antenna misplacement sensitivity study.

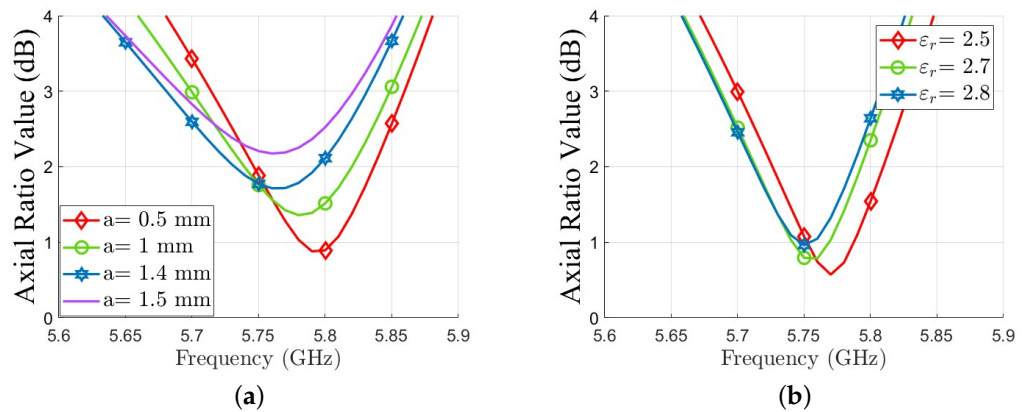


Figure 16. Simulated results for the sensitivity analysis. (a) Displacement error. (b) Permittivity uncertainty.

Another explanation for the differences between simulation and measurement is what the printer understands when working with different infill percentages. Since the box as shown above has a very low infill, it is likely that the printer does not differentiate between a 15% infill and a 10% infill, thus affecting the permittivity of the box. For this, Figure 16b shows a sensitivity study of slight variations in the permittivity of the box, showing that the antenna is not sensitive to those variations.

## 6. Conclusions

This study presented the development of a 3D-printed enclosed twist dielectric resonator antenna (DRA) designed to achieve circular polarization at a center frequency of 5.8 GHz. The design focused on meeting the requirements of unmanned aerial vehicle (UAV) applications, specifically in terms of bandwidth, gain, and compact volume.

The results obtained from both simulation and measurement confirm that the antenna performs effectively in these areas, demonstrating that 3D printing can be a viable approach to producing antennas for UAV applications. The manufactured antenna achieved the

desired circular polarization and bandwidth characteristics, as well as adequate gain. However, several manufacturing and design challenges were encountered throughout the development process due to the inherent sensitivities associated with these antennas. Therefore, it is important to assess the materials and dimensionality of the antenna for their implementation.

**Author Contributions:** Conceptualization, A.Á.-S. and F.P.; methodology, F.P.; validation, A.Á.-S., M.D. and F.P.; investigation, A.Á.-S.; resources, F.P. and M.D.; writing—original draft preparation, A.Á.-S., M.D. and F.P.; writing—review and editing, A.Á.-S., M.D. and F.P.; funding acquisition, F.P. All authors have read and agreed to the published version of the manuscript.

**Funding:** This work was partially funded by ANID FONDEQUIP EQM220109, FONDECYT REGULAR 1221090, FONDEF IDeA ID23I10360, Anillo ATE220057 and ONRG N62909-23-1-2016.

**Institutional Review Board Statement:** Not applicable.

**Informed Consent Statement:** Not applicable.

**Data Availability Statement:** The datasets used and analyzed during the current study are available from the corresponding author upon reasonable request.

**Acknowledgments:** The authors would like to thank the Universidad Técnica Federico Santa María, Chile, for the measurements in the anechoic chamber.

**Conflicts of Interest:** The authors declare no conflicts of interest.

## References

1. Whittaker, T.; Zhang, S.; Powell, A.; Stevens, C.J.; Vardaxoglou, J.Y.C.; Whittow, W. 3D Printing Materials and Techniques for Antennas and Metamaterials: A survey of the latest advances. *IEEE Antennas Propag. Mag.* **2023**, *65*, 10–20. [CrossRef]
2. Premix Preperm Website. Available online: <https://www.preperm.com> (accessed on 2 September 2023).
3. Wang, Y.; Zhang, X.; Su, R.; Chen, M.; Shen, C.; Xu, H.; He, R. 3D Printed Antennas for 5G Communication: Current Progress and Future Challenges. *Chin. J. Mech. Eng. Addit. Manuf. Front.* **2023**, *2*, 100065. [CrossRef]
4. Numan, A.B.; Sharawi, M.S. Extraction of Material Parameters for Metamaterials Using a Full-Wave Simulator [Education Column]. *IEEE Antennas Propag. Mag.* **2013**, *55*, 202–211. [CrossRef]
5. Isakov, D.; Lei, Q.; Castles, F.; Stevens, C.; Grovenor, C.; Grant, P. 3D printed anisotropic dielectric composite with meta-material features. *Mater. Des.* **2016**, *93*, 423–430. [CrossRef]
6. Olivová, J.; Popela, M.; Richterová, M.; Štefl, E. Use of 3D Printing for Horn Antenna Manufacturing. *Electronics* **2022**, *11*, 1539. [CrossRef]
7. Castillo-Tapia, P.; Rico-Fernández, J.; Clendinning, S.; Mesa, F.; Quevedo-Teruel, O. Evaluation of Losses in 3-D-Printed Geodesic Lenses Using a Ray-Tracing Model. *IEEE Trans. Antennas Propag.* **2024**, *72*, 234–242. [CrossRef]
8. Shin, S.H.; Shang, X.; Ridler, N.M.; Lucyszyn, S. Polymer-Based 3-D Printed 140–220 GHz Low-Cost Quasi-Optical Components and Integrated Subsystem Assembly. *IEEE Access* **2021**, *9*, 28020–28038. [CrossRef]
9. Nikkhah, A.; Oraizi, H. Implementation of Parasitic DRA Elements for Improvement of Circular Polarization. *IEEE Antennas Wirel. Propag. Lett.* **2021**, *20*, 2387–2391. [CrossRef]
10. Petosa, A. *Dielectric Resonator Antenna Handbook*; Artech: Boston, MA, USA, 2007.
11. Cuevas, M.; Pizarro, F.; Leiva, A.; Hermosilla, G.; Yunge, D. Parametric Study of a Fully 3D-Printed Dielectric Resonator Antenna Loaded With a Metallic Cap. *IEEE Access* **2021**, *9*, 73771–73779. [CrossRef]
12. Leszkowska, L.; Rzymowski, M.; Nyka, K.; Kulas, L. High-Gain Compact Circularly Polarized X-Band Superstrate Antenna for CubeSat Applications. *IEEE Antennas Wirel. Propag. Lett.* **2021**, *20*, 2090–2094. [CrossRef]
13. Manabe, T.; Miura, Y.; Ihara, T. Effects of antenna directivity and polarization on indoor multipath propagation characteristics at 60 GHz. *IEEE J. Sel. Areas Commun.* **1996**, *14*, 441–448. [CrossRef]
14. Syrytsin, I.; Zhang, S.; Pedersen, G.F.; Ying, Z. User Effects on the Circular Polarization of 5G Mobile Terminal Antennas. *IEEE Trans. Antennas Propag.* **2018**, *66*, 4906–4911. [CrossRef]
15. Nielsen, J.O.; Pedersen, G.F. Dual-polarized indoor propagation at 26 GHz. In Proceedings of the 2016 IEEE 27th Annual International Symposium on Personal, Indoor, and Mobile Radio Communications (PIMRC), Valencia, Spain, 4–8 September 2016; pp. 1–6. [CrossRef]

16. Diaz, S.; Diaz, M.; Rajo-Iglesias, E.; Pizarro, F. Circular polarized 3D-printed cylindrical DRA using parasitic dielectric helix. *Sci. Rep.* **2023**, *13*, 11838. [[CrossRef](#)] [[PubMed](#)]
17. Przepiorowski, J.; Munina, I.; Ammann, M.J. 3D-Printed Beam-Switching Dielectric Resonator Antenna with an Integrated Polarizer. In Proceedings of the 2024 International Conference on Electromagnetics in Advanced Applications (ICEAA), Lisbon, Portugal, 2–6 September 2024; pp. 291–294. [[CrossRef](#)]
18. Xia, Z.X.; Leung, K.W. 3-D-Printed Wideband Circularly Polarized Dielectric Resonator Antenna With Two Printing Materials. *IEEE Trans. Antennas Propag.* **2022**, *70*, 5971–5976. [[CrossRef](#)]
19. Avila, A.; Diaz, M.; Pizarro, F. Circular Polarized 3D-Printed Enclosed Twist Dielectric Resonator Antenna. In Proceedings of the 2023 IEEE International Symposium on Antennas and Propagation and USNC-URSI Radio Science Meeting (USNC-URSI), Portland, ON, USA, 23–28 July 2023; pp. 701–702. [[CrossRef](#)]
20. Luk, K.; Leung, K. *Dielectric Resonator Antennas*; Research Studies Press: Baldock, UK, 2003.
21. Pattnaik, S.; Sahu, S.; Dash, S.K.K.; Behera, S.S. Rotated stacked dielectric resonator antenna with sierpinski fractal for circular polarization. In Proceedings of the 2015 International Conference on Communications and Signal Processing (ICCSPP), Melmaruvathur, India, 2–4 April 2015; pp. 0361–0364. [[CrossRef](#)]
22. Gotra, S.; Varshney, G.; Yaduvanshi, R.S.; Pandey, V.S. Dual-band circular polarisation generation technique with the miniaturisation of a rectangular dielectric resonator antenna. *IET Microwaves Antennas Propag.* **2019**, *13*, 1742–1748. [[CrossRef](#)]
23. Abd Rahman, N.A.; Mohd Yasin, M.N.; Ibrahim, I.M.; Jusoh, M.; Noor, S.K.; Eksalin Emalda Mary, M.R.; Zamin, N.; Nurhayati, N. A Review of Circularly Polarized Dielectric Resonator Antennas: Recent Developments and Applications. *Micromachines* **2022**, *13*, 2178. [[CrossRef](#)]
24. Bjorkqvist, O.; Zetterstrom, O.; Quevedo-Teruel, O. Additive manufactured dielectric Gutman lens. *Electron. Lett.* **2019**, *55*, 1318–1320. [[CrossRef](#)]
25. Nicolson, A.M.; Ross, G.F. Measurement of the Intrinsic Properties of Materials by Time-Domain Techniques. *IEEE Trans. Instrum. Meas.* **1970**, *19*, 377–382. [[CrossRef](#)]

**Disclaimer/Publisher’s Note:** The statements, opinions and data contained in all publications are solely those of the individual author(s) and contributor(s) and not of MDPI and/or the editor(s). MDPI and/or the editor(s) disclaim responsibility for any injury to people or property resulting from any ideas, methods, instructions or products referred to in the content.